

AD-A250 959



1

Solution of Potential Problems Using a Spectral Boundary Integral Method

J. Huh and W.W. Schultz
Department of Mechanical Engineering and Applied Mechanics

Contract Number N00014-86-K-0684
Technical Report No. 89-02

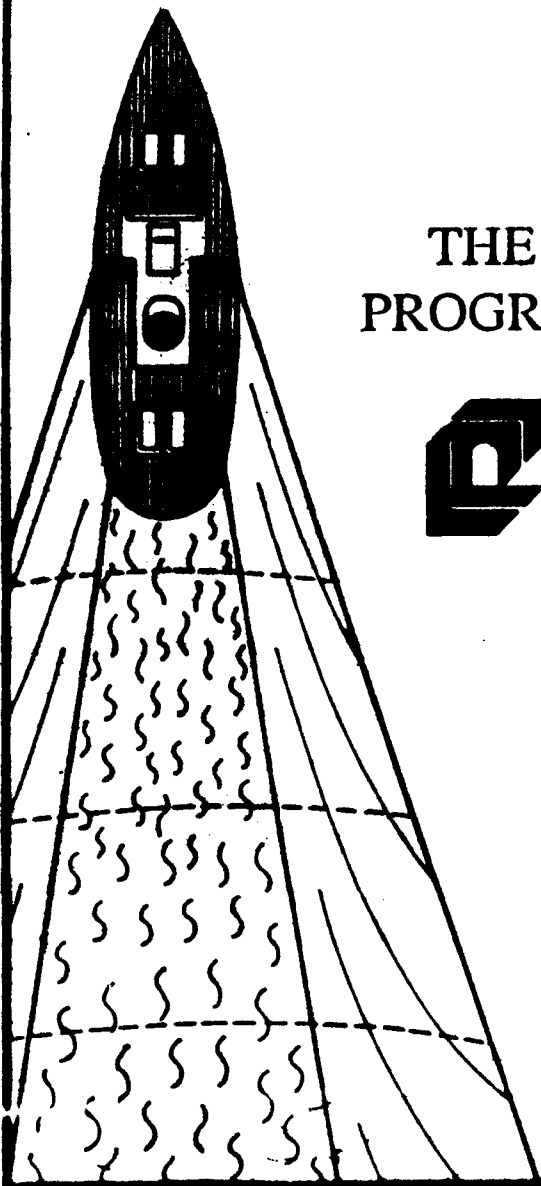
March, 1989

DISTRIBUTION STATEMENT A
Approved for public release;
Distribution Unlimited

DTIC
ELECTE
JUN 1 1992
S C D

92-13782

92 5 26 008



**THE UNIVERSITY OF MICHIGAN
PROGRAM IN SHIP HYDRODYNAMICS**



COLLEGE OF ENGINEERING

**NAVAL ARCHITECTURE &
MARINE ENGINEERING**

AEROSPACE ENGINEERING

**MECHANICAL ENGINEERING &
APPLIED MECHANICS**

**SHIP HYDRODYNAMIC
LABORATORY**

**SPACE PHYSICS RESEARCH
LABORATORY**



Abstract

The advantages of solving two-dimensional potential problems using spectral boundary integral methods are examined. Using fast Fourier transforms, we expand the spatial coordinates x and y using an arclength parameter s . This spectral representation is very accurate when the geometry is smooth and nodal spacing is uniform. Two spectral formulations are outlined. One is based on Baker's [11] integration scheme at every other node to avoid the kernel singularities, and the other is based on the kernel desingularization of Roberts [12]. An error analysis and convergence studies for several geometries are shown.

Statement A per telecon
Dr. Edwin Rood ONR/Code 1132
Arlington, VA 22217-5000

NWW 6/1/92

3 *



*page 2 intentionally missing

Accession For	
NTIS GRA&I	<input checked="" type="checkbox"/>
NTIS TAB	<input type="checkbox"/>
Unannounced	<input type="checkbox"/>
Justification	
By _____	
Distribution/	
Availability Codes	
Dist	Avail and/or Special
A-1	

1 Introduction

Boundary integral methods and spectral methods are two of the most powerful techniques in computational mechanics. In this paper we combine these approaches to obtain a very accurate algorithm for potential problems. The governing equation for potential problems is elliptic, requiring one condition on the enclosing boundary. The boundary integral method only solves for an unknown on the boundary, which reduces the effective dimension of the potential problem by one and significantly decreases the computational effort unless the contour is highly distorted. In addition, if we use spectral representation for the boundary values, we may get exponentially accurate solutions.

The solutions of two-dimensional potential problems can be described by a complex analytic function. The boundary integral method can then be derived from Cauchy's integral theorem (Greenhow, Vinje, Brevig, and Taylor [1], Vinje and Brevig [2], Lai and Hromadka [3]), rather than the more general method using a free-space Green's function (Longuet-Higgins and Cokelet [4]). Applying the real and imaginary parts of the Cauchy integral theorem results in two real algebraic systems. While Cauchy's integral and the Green's function formulations are not directly compared here, Dold and Peregrine [5,6] indicate that the former method [1,2,3] is clearly superior. Schultz [7,8] shows that the error of the complex formulation can be reduced by solving these two systems of equations in a least-square sense for nonlinear breaking wave simulations. Schultz and Hong [9] compare the results for the overdetermined, strong, and weak systems using a piecewise-linear

method. They concluded that the overdetermined system is superior to others in many cases.

In general, an integral equation is solved by a numerical model that assumes the boundary is composed of piecewise-polynomial curves (panels) and the known and unknown boundary values are approximated as piecewise-continuous functions along the boundary. Most complex variable boundary integral methods adopt piecewise-linear representations of the complex functions. A linear interpolation then results in second-order accurate integration and typically gives second-order accurate solutions for the boundary integral solution as well. To improve accuracy, we expand the known and unknown boundary values and the boundary shape in a global Fourier series using an arclength parameter. Spectral methods then result in exponentially accurate integration and give exponentially accurate solutions.

In this paper, two spectral formulations are outlined. One is based on Baker's [11] integration at every other node point to avoid the kernel singularities, and the other is based on the kernel desingularization of Roberts [12]. The advantages of the spectral boundary integral method are discussed, and the error is analyzed and compared to piecewise-linear method for several test cases. The test cases show the effects of geometric curvature, nodal spacing, and local solution gradients on the solution error.

2 Problem Formulation

Figure 1 shows the problem domain with the bounding surface ∂R . Solutions of potential problems ϕ and ψ can be written as

$$\beta(z) = \phi + i\psi. \quad (1)$$

Here, $z = x + iy$ represents the two spatial coordinates. Cauchy's theorem then gives

$$\oint_{\partial R} \frac{\beta(z)}{z - \zeta_k} dz = i\alpha\beta(\zeta_k), \quad (2)$$

where α is 0 or 2π if the location of the kernel singularity, ζ_k , is outside or inside the boundary, respectively. If the kernel singularity is on the boundary ($\zeta_k \in \partial R$), α is the included angle, and (2) is treated as a principal value integral.

Our goal is to convert (2) into an algebraic system as in Schultz and Hong [9]. The algebraic system is formed by discretizing the integral and letting the kernel singularity approach each of the N nodal points, $\zeta_k \rightarrow z_k$. A special limiting process is then needed to evaluate the integration near ζ_k .

2.1 Spectral Method I

Following the method outlined by Baker [11], exponential convergence can be achieved by evaluating the principal value integral of (2) using the trapezoidal rule. To obtain this convergence, the integral must be periodic and integrated with respect to a real variable, in this case, an arclength parameter, s . The integral

becomes

$$\oint \frac{\beta(s)}{z(s) - z_k} \frac{dz}{ds} ds = i\pi\beta(z_k). \quad (3)$$

Baker [11] indicates this expression will give exponentially convergent results when trapezoidal integration is used for a smooth, periodic integrand and the shape (and hence dz/ds) is known exactly. In contour dynamics problems, for example, the bounding surface ∂R must be calculated from evolution equations. However, if the contour is known to be smooth, $z(s)$ and hence dz/ds can be determined with exponential accuracy if spectral methods are used. We have performed these calculations using a standard fast Fourier transform (FFT) routine for both $x(s)$ and $y(s)$ to obtain exponential accuracy.

In (3), the integrand is singular as z approaches z_k . The singular part of the integral is avoided to smooth the integrand by evaluating the principal-value integral at every other point. The algebraic equations can be written as

$$\sum_{j=1}^N \Gamma_{jk} \beta(s_j) = 0 \quad \text{for } k = 1 \dots, N, \quad (4)$$

where

$$\Gamma_{jk} = \begin{cases} \frac{1}{z_j - z_k} \left(\frac{dz}{ds} \right)_j & \text{if } |j - k| \text{ is odd} \\ -i\pi & \text{if } j = k \\ 0 & \text{if } |j - k| \text{ is even and } j \neq k. \end{cases} \quad (5)$$

If ϕ is given on the boundary, ψ can be calculated from (4) and (5). Since the integration is carried out at every other point, unlike the piecewise-linear representation of [9], many Γ_{jk} are zero (nearly one-half). Obviously, this saves much time (nearly one-half) in solving the algebraic system.

2.2 Spectral Method II

Roberts [12] used a desingularized kernel in his vortex formulation. Generally, it is difficult to find a suitable desingularized form of a kernel in an integral equation, but in the complex formulation it is relatively simple. The Cauchy integral equation (3) can be easily rewritten as

$$\oint \frac{\beta(s) - \beta(z_k) dz}{z(s) - z_k ds} = 0, \quad (6)$$

where the principal value integral can be replaced by the closed contour integral since the integrand is no longer singular. When z approaches z_k , the integrand approaches $d\beta/ds$ at the k th node. Therefore, this kernel does not exhibit singular behavior as z approaches z_k . Integral equation (6) is converted to the following sets of equations for $k = 1 \dots N$:

$$\sum_{j=1, j \neq k}^N \frac{\beta_j - \beta_k}{z_j - z_k} \left(\frac{dz}{ds}\right)_j + \left(\frac{d\beta}{ds}\right)_k = 0 \quad \text{for } k = 1, \dots, N, \quad (7)$$

where N is the number of nodes. The desingularized algebraic system (7) requires the derivative of β and hence effectively becomes a differential system. To evaluate these derivatives spectrally, we use a trigonometric interpolation of β [13]:

$$\beta(s) = \sum_{j=1}^N C_j(s) \beta_j, \quad (8)$$

where

$$C_j = \frac{1}{N} \sin \pi(s - s_j) \cot \frac{\pi}{N}(s - s_j), \quad (9)$$

and the derivative of C_j is

$$\frac{dC_j}{ds}(s_i) = \begin{cases} \frac{\pi}{N} (-1)^{i+j} \cot \frac{\pi}{N}(s_i - s_j) & \text{if } i \neq j \\ 0 & \text{if } i = j. \end{cases} \quad (10)$$

Then, (7) becomes

$$\sum_{j=1}^N \Gamma_{jk} \beta_j = 0 \quad \text{for } k = 1, \dots, N, \quad (11)$$

where the influence coefficients Γ_{jk} are now

$$\Gamma_{jk} = \begin{cases} \frac{1}{x_j - x_k} \left(\frac{dx}{ds} \right)_j + \frac{dC_i}{ds}(s_k) & \text{if } j \neq k \\ - \sum_{i=1, i \neq k}^N \frac{1}{x_i - x_k} \left(\frac{dx}{ds} \right)_i & \text{if } j = k. \end{cases} \quad (12)$$

Unlike spectral method I, the desingularized kernel is evaluated at every nodal point, and hence the matrix is full.

3 Numerical Investigation

Comparisons of accuracy, convergence rate, and computing time are made for spectral method I, spectral method II, and the piecewise-linear method. The effects of nonuniform nodal spacing, contour shape, and nearly singular solution characteristics on the solution error are investigated.

To solve the matrix problem, a conjugate gradient iterative technique is used. This technique solves the problem in an order of UVL operations, where U is the number of unknowns, V is the number of equations, and L is the number of iterations. The computational savings of the iterative technique would be important if time marching were desired, especially since a good initial guess is available from the previous time step. However, even with a homogeneous initial guess, a typical solution for a nonsingular matrix requires less than 10 iterations.

According to Schultz and Hong [9], the overdetermined system for the piecewise-linear method is generally most accurate, and the convergence rate of the overdetermined system can be twice that of the weak or strong algebraic systems. Similarly, the real and imaginary parts of (5) for spectral I and (12) for spectral II can be imposed as well. Although we find that for uniformly spaced nodes the convergence rates of both spectral methods are nearly identical for all algebraic systems, the overdetermined system gives more stable results for distorted contours and nonuniform nodal spacing [14]. We use an overdetermined system for all methods unless otherwise indicated.

The test function is $\beta = \sin z$ unless otherwise stated. The real part of β , i.e., ϕ , is prescribed at each node; ψ is then determined from the boundary integral method and compared to the known $Im(\beta)$. We perform all calculations on an Apollo DN4000 Workstation using double precision (16 digits).

3.1 Rate of Convergence and Computing Time

The root mean square errors, E_2 , evaluated at the nodal points and the corresponding computing times are examined as a function of the number of nodes to determine convergence rates and computational efficiency. Figure 2 compares E_2 for uniformly spaced nodes on a circular contour for three methods: spectral I, spectral II, and piecewise-linear. The spectral methods are much more accurate than the piecewise-linear method, and spectral II is slightly better than spectral I.

The effect of the contour shape on the efficiency is examined for elliptic contours with various eccentricities ($e = 0.0$ to 0.995). The diameter of the major axis is fixed at 2.0 and centered on the x axis. Figure 3 shows solutions for various elliptic contours when N is 16 . Here, the arclength parameter spacing is determined by $\Delta s = r\Delta\theta$, where $\Delta\theta$ is constant. As the eccentricity increases, the E_2 of spectral I is nearly constant up to $e = 0.7$ and then increases rapidly; that of spectral II also remains nearly constant for small e but decreases at $e = 0.7$.

The nodal spacing s varies as the eccentricity increases, and the integration near the singular point is not accurate using spectral I, which explains the increase in E_2 after $e = 0.7$. On the other hand, the integrand in spectral I has a limiting form as z goes to z_k . Therefore, E_2 is independent of eccentricity. Both spectral methods are much more accurate than the piecewise-linear method except near $e = 1$, where the piecewise-linear method is more accurate than spectral I.

In Figure 4, error vs. CPU time is shown for an elliptic contour ($e = 0.866$). Generally the CPU time of spectral I is the smallest for a given N , although the greater accuracy of spectral II makes it more computationally efficient. Figure 4 clearly shows that both spectral methods are more efficient than the piecewise-linear method.

3.2 Nonuniform Nodal Spacing

Sometimes nonuniform nodal spacing is desirable, as when solution refinement is needed due to large solution gradients. The nodal spacing also varies in problems with convective nodes such as free surface flow problems. This can cause numerical instabilities, requiring a filtering or a regriding scheme to maintain uniform spacing.

In the previous section, we note that as ϵ increases, the nodal spacing about an arclength varies, but the accuracy remains good for spectral II. In those cases, even though the nodal spacing about the arclength is nonuniform, its variation is very smooth and the nodal spacing about θ is uniform. However, if only one node is moved, the abrupt change in nodal spacing seriously affects the fast Fourier transform accuracy. Here, two cases are considered: one when an abrupt change occurs in nodal spacing, and the other when the nodal spacing varies slowly.

The first case is shown in Figure 5 for a circular contour. When node 1 is moved a fraction p of the uniform nodal spacing $\Delta\theta = 2\pi/N$ towards node 2, then the accuracy decreases rapidly as p increases for all methods. Figure 5 compares the results of the three methods when p is 0.1. For $N > 16$, the piecewise-linear method gives the most accurate solution, and for all N , spectral II gives more accurate solutions than spectral I, as expected. Figure 6 compares the results for various p when N is 16. Near $p = 0$, the spectral methods give more accurate results than the piecewise-linear method, and the accuracy increases rapidly for $0 \leq p \leq 0.1$. But as p increases, the spectral methods become inaccurate. The accuracy of the

piecewise-linear method does not degrade as significantly as p increases.

We conclude that the piecewise-linear method is less susceptible to an abrupt change of nodal spacing. The inaccuracies of the spectral methods are due to integration errors as well as FFT routine errors. Integration errors affect the accuracy of spectral I more significantly than spectral II because singular contribution on the integral doesn't cancel for uneven nodal spacing in spectral I, while FFT routine errors affect the accuracy of both spectral methods. Hence spectral II can tolerate larger nodal spacing irregularities than spectral I.

The second case is shown in Figure 7, which compares the results of the three methods for an elliptic contour of slowly varying nodal spacing. Here, $\Delta\theta$ varies as a cosine function, b is the amplitude of the cosine function, and $N = 32$. Both spectral methods are more accurate than the piecewise-linear method, and spectral method II is significantly better than spectral I.

3.3 Distorted Contours

The computational domain can become very distorted. For example, in wave modulation problems, long waves are combined with short waves. After conformal mapping, a contour similar to the following is obtained:

$$x = r(\theta) \cos \theta ,$$

$$y = r(\theta) \sin \theta ,$$

$$r(\theta) = 1 + a \cos k\theta .$$

In Figure 8, the domain geometry is shown when k is 8. Figure 9 compares the results of the three methods. In this case, spectral II gives the most accurate results, and when $N \geq 128$, spectral I is more accurate than the piecewise-linear method. Figures 10 and 11 show the results for different k using spectral I and spectral II, respectively. As expected, as k increases, the accuracy decreases, because the domain geometry is more contorted. Figure 12 compares the three methods for varying a when k is 8 and N is 64. When $a = 0$ (circular contour), both spectral methods are more accurate than the piecewise-linear method, as shown previously. As a increases, E_2 in spectral I increases rapidly, and when $a \geq 0.1$, the accuracy of spectral I is worse than that of the piecewise-linear method. In spectral II, the E_2 also increases, but the accuracy is still better than the piecewise-linear method. From these test cases, spectral II is shown to be the most efficient method for distorted contours.

The boundary integral accuracy is known to deteriorate in the vicinity of contour corners due to the infinite geometric curvature (Schultz and Hong [9]). With spectral methods, since the FFT for $x(s)$ and $y(s)$ converges very slowly, our results show very poor results. Therefore, we conclude that spectral methods offer no advantages for contours with corners. The results are not shown here.

3.4 Desingularization

We use the same strategy for the locating the kernel singularities outside the contour as Schultz and Hong [9]. The strategy uses the perpendicular bisector of the straight contour between adjacent nodes. This method has two potential difficulties, as pointed out by Schultz and Hong [9]: if f is too small, the singular point may lie inside a convex contour, but if f is too large, the singular point may lie inside the domain of a highly contorted contour.

Figure 13 shows the error computed for several values of f in spectral I, where the nodes are placed evenly on a circular contour with $\beta = \sin z$. Figure 14 shows the error computed for various values of f in spectral I where N is 16. In this case, since the desingularized kernel is used, integration is carried out at every point. Generally, the algebraic system becomes less diagonally dominant as f increases, requiring more iterations and a tighter tolerance on the convergence parameter to achieve the desired accuracy.

4 Conclusions

Our numerical investigation shows that the spectral II is the most efficient and accurate in almost all cases. For smooth contours with uniform nodal spacing, both spectral methods are more accurate than the piecewise-linear method. The piecewise-linear method is less susceptible to an abrupt change in the nodal spac-

ing than spectral methods, but when the nodal spacing varies slowly, spectral II is most accurate. For distorted contours, spectral II is the most efficient method, because it gives more accurate results for the same N . Both spectral methods have difficulties handling contours with corners. As for efficiency, both spectral methods need less computing time than the piecewise-linear method, and spectral II is the fastest scheme. The accuracy of spectral II may be further improved by filtering or a node redistribution scheme, especially when discontinuities in nodal spacing or contour shape are encountered.

The spectral approach may be extended to periodic three-dimensional potential problems using integral equations derived from Green's theorem or the normal derivative of Green's theorem. Hence, the spectral boundary integral method may yield greater efficiency and accuracy for three-dimensional problems as well.

Acknowledgements

This work was partially supported by the Program in Ship Hydrodynamics at The University of Michigan, funded by the University Research Initiative of the Office of Naval Research, Contract No. N000184-86-K-0684. The authors acknowledge S. W. Hong and S. W. Joo for their helpful discussions and suggestions.

References

1. M. Greenhow, T. Vinje, P. Brevig, and J. Taylor, *J. Fluid Mech.* **118**, (1982).
2. T. Vinje and P. Brevig, *Adv. Water Resources*, (1981).
3. C. Lai and T. V. Hromadka II, in *Proceedings of ASCE Hydraulic Division Specialty Conference*, Orlando, Florida, (1985).
4. M. S. Longuet-Higgins and E. D. Cokelet, *Proc. Royal Soc. London A*, **350**, (1976).
5. J. W. Dold and D. H. Peregrine, School of Mathematics, Univ. of Bristol, Report AM-84-04, (1984).
6. J. W. Dold and D. H. Peregrine, *Numerical Methods for Fluid Dynamics II*, Oxford U.P., (1986).
7. W. W. Schultz, in *Proceedings of 11th IMACS World Congress, 2*, Oslo, Norway, (1985).
8. W. W. Schultz, in *Proceedings of 16th ONR Symposium on Naval Hydrodynamics*, Berkeley, California, (1986).
9. W. W. Schultz and S. W. Hong, to appear in *J. Comp. Physics*, (1988).
10. G. R. Baker, D. I. Meiron and S. A. Orszag, *J. Fluid Mech.* **123**, (1982).
11. G. R. Baker, *Waves on Fluid Interfaces*, Academic Press, (1983).
12. A. J. Roberts, *IMA J. Appl. Math.* **31**, (1983).

13. J. Boyd, *Spectral Methods*, Springer-Verlag, (1989).
14. W. W. Schultz and J. Huh, to appear in *4th International Workshop on Water Waves and Floating Bodies*, Norway, (1989).

LIST OF SYMBOLS

- a : amplitude of cosine variation of $r(\theta)$ in complicated contour
- b : amplitude of cosine variation of $\Delta\theta$
- E_2 : root mean square error
- e : eccentricity of an ellipse, $\sqrt{A^2 - B^2}/A$, A = long axis, B = short axis
- f : desingularization parameter for locating kernel singular point
- I_{jk} : discretized kernel
- k : number of bumps in complicated contour
- N : total number of nodes
- p : amounts of uniform $\Delta\theta$ moving from node 1 to node 2
- R : domain of the problem
- s : curvilinear coordinate on the contour
- U, V : row and column number of an overdetermined matrix
- $x(s), y(s)$: x and y coordinate of the contour
- z : complex coordinate of a point
- z_j : j^{th} node
- Greek Letters**
- α : a constant (alpha)
- β : complex potential (beta)
- Γ_{jk} : integral equation influence coefficient (upper case Gamma)
- ζ_k : k^{th} control point (zeta)

θ : tangent angle of the contour with positive x-axis (theta)
 ϕ : real part of β (phi)
 ψ : imaginary part of β (psi)
 ∂R : contour of computing domain

LIST OF FIGURES

- Figure 1 Domain and Bounding Surfaces
- Figure 2 Comparisons of Truncation Error Convergence
(overdetermined system, $\beta = \sin(z)$, ϕ is given, circular contour)
solid line : spectral I, dashed line : spectral II, dotted line : piecewise-linear method
- Figure 3 Comparisons of E_2 Errors for Various e
($N=16$, overdetermined system, $\beta = \sin(z)$, ϕ is given, elliptic contour)
solid line : spectral I, dashed line : spectral II, dotted line : piecewise-linear method
- Figure 4 Comparisons of Relations between E_2 Errors and Computing Times
(overdetermined system, $\beta = \sin(z)$, ϕ is given, elliptic contour, $e = 0.866$)
solid line : spectral I, dashed line : spectral II, dotted line : piecewise-linear method
- Figure 5 Comparisons of E_2 Errors (An Abrupt Change in Nodal Spacing)
($p = 0.1$, overdetermined system, $\beta = \sin(z)$, ϕ is given, circular contour)
solid line : spectral I, dashed line : spectral II, dotted line : piecewise-linear method
- Figure 6 Comparisons of E_2 Errors for Various p (An Abrupt Change in Nodal Spacing)
($N=16$, overdetermined system, $\beta = \sin(z)$, ϕ is given, circular contour)
solid line : spectral I, dashed line : spectral II, dotted line : piecewise-linear method
- Figure 7 Comparisons of E_2 Errors for Various b (Slowly Varying Nodal Spacing)
($N=32$, overdetermined system, $\beta = \sin(z)$, ϕ is given, elliptic contour, $e = 0.866$)

solid line : spectral I, dashed line : spectral II, dotted line : piecewise-linear method

Figure 8 Geometry of Complicated Contours

($x = r \cos \theta$, $y = r \sin \theta$, $r = 1 + a \cos k\theta$, $k = 8$, $a = 0.1$)

Figure 9 Comparisons of Truncation Error Convergence

($a = 0.1$, overdetermined system, $\beta = \sin(z)$, ϕ is given, complicated contour)

solid line : spectral I, dashed line : spectral II, dotted line : piecewise-linear method

Figure 10 Truncation Error Convergence for Various k

(spectral I, $a = 0.1$, overdetermined system, $\beta = \sin(z)$, ϕ is given, complicated contour)

solid line : $k = 6$, dashed line : $k = 8$, dotted line : $k = 10$

Figure 11 Truncation Error Convergence for Various k

(spectral II, $a = 0.1$, overdetermined system, $\beta = \sin(z)$, ϕ is given, complicated contour)

solid line : $k = 6$, dashed line : $k = 8$, dotted line : $k = 10$

Figure 12 Truncation Error Convergence for Various a

(spectral II, $k = 8$, overdetermined system, $\beta = \sin(z)$, ϕ is given, complicated contour)

Figure 13 Comparisons of Truncation Error Convergence (Desingularization)

(spectral I, overdetermined system, $\beta = \sin(z)$, ϕ is given, circular contour)

solid line : original, dashed line : $f = 1$, dotted line : $f = 3$

Figure 14 Effect of Desingularization Parameter on Error

($N=16$, spectral I, overdetermined system, $\beta = \sin(z)$, ϕ is given, circular contour)

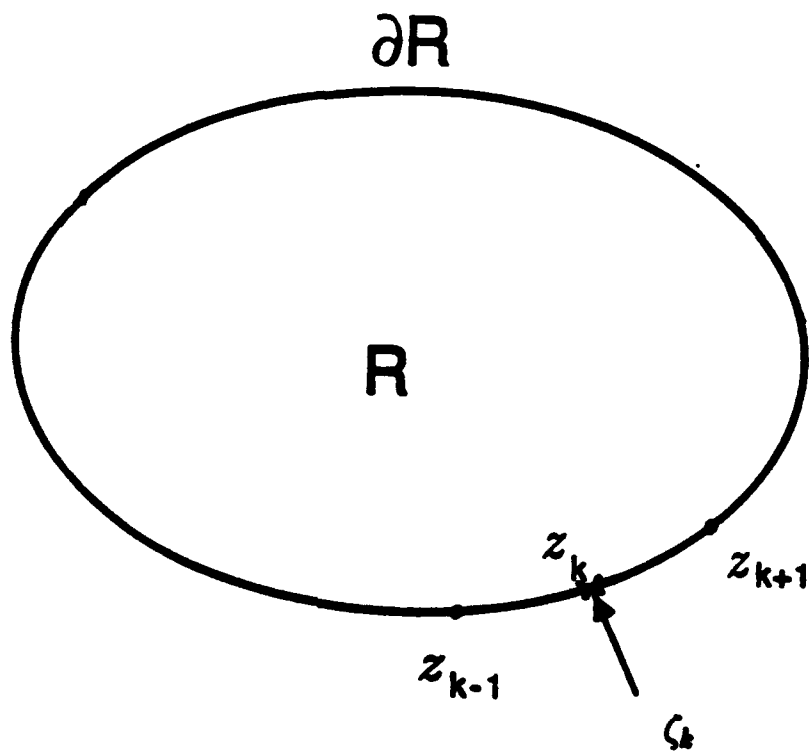


Figure 1

Figure 2

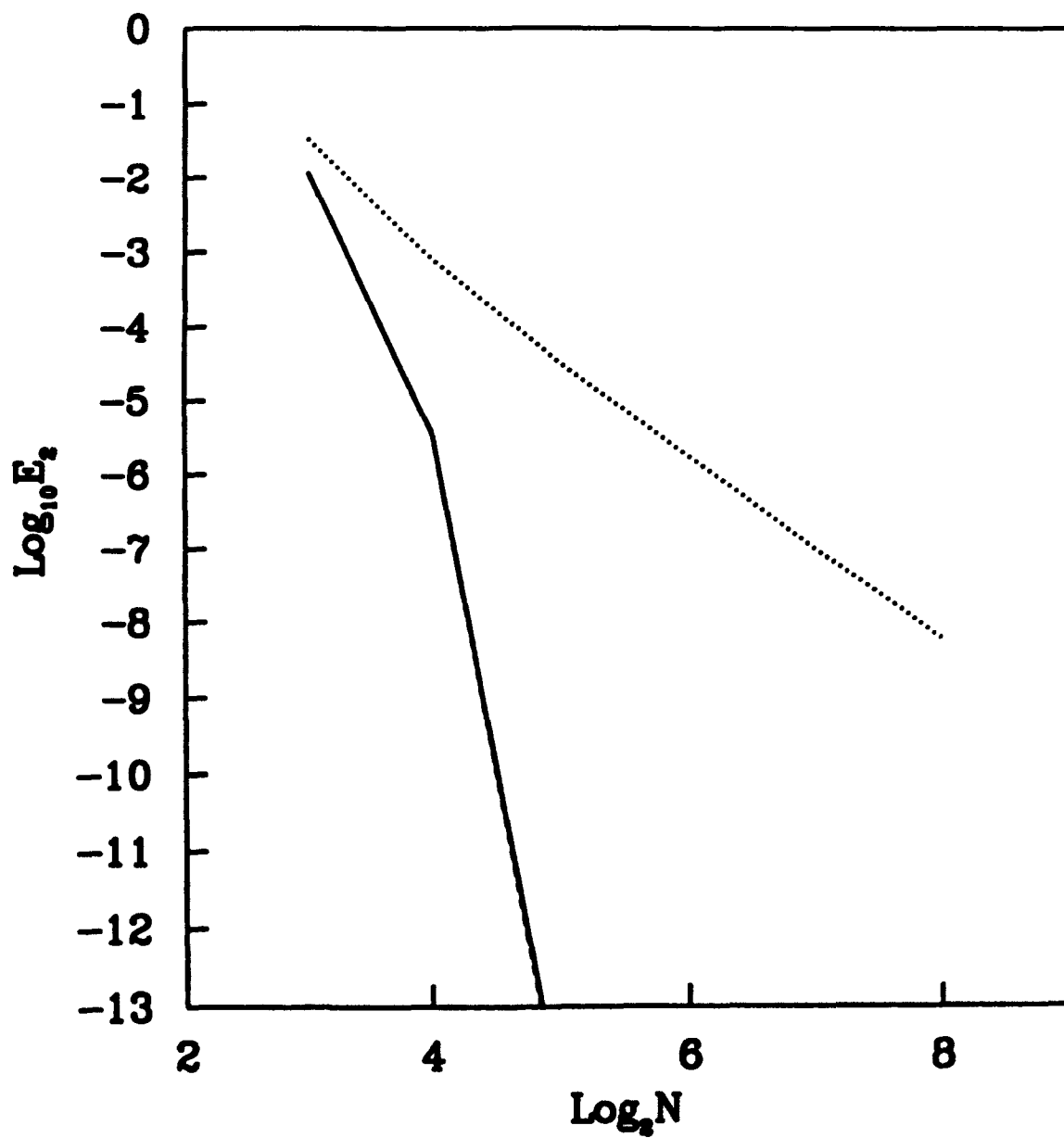


Figure 3

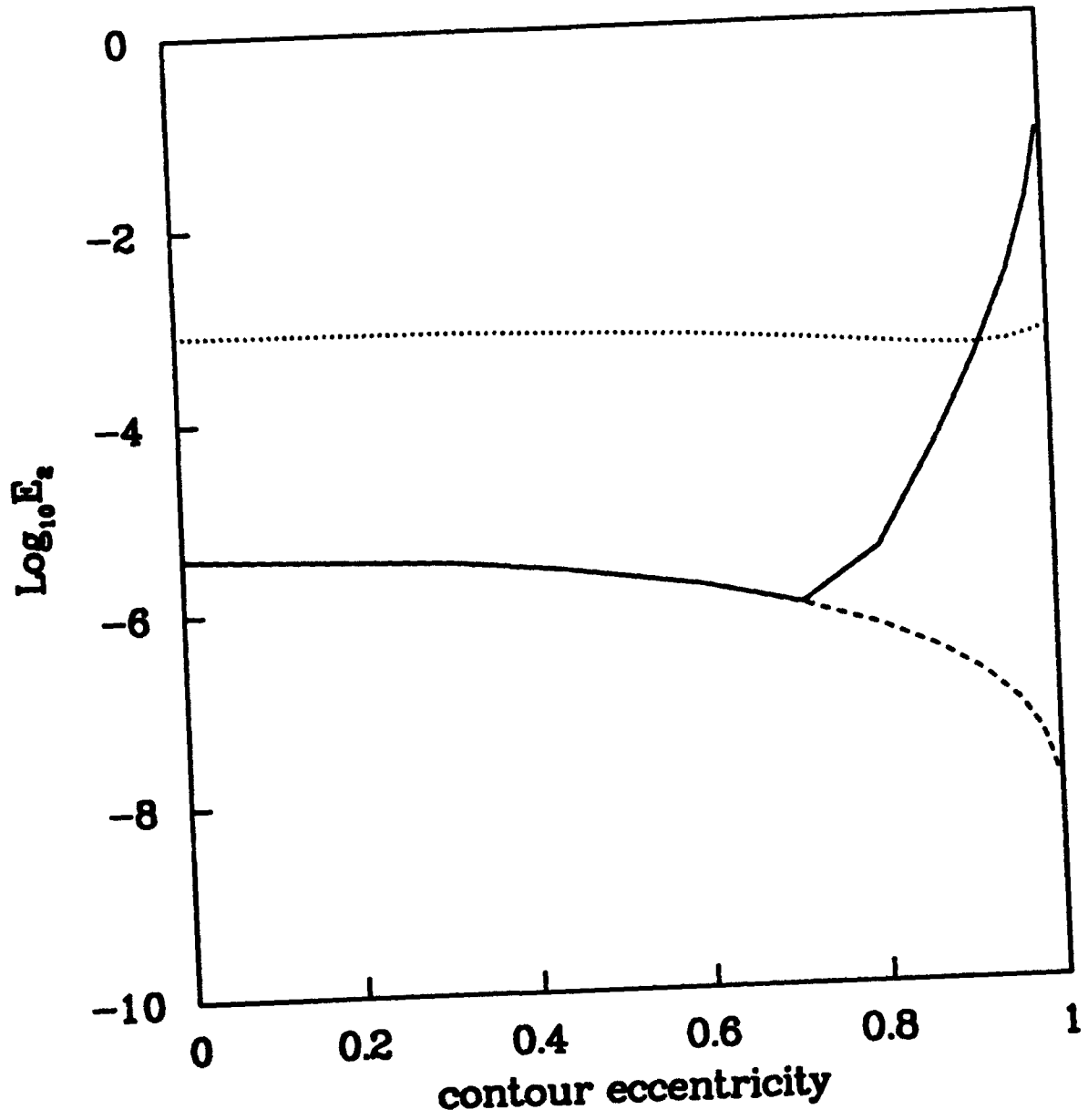


Figure 4

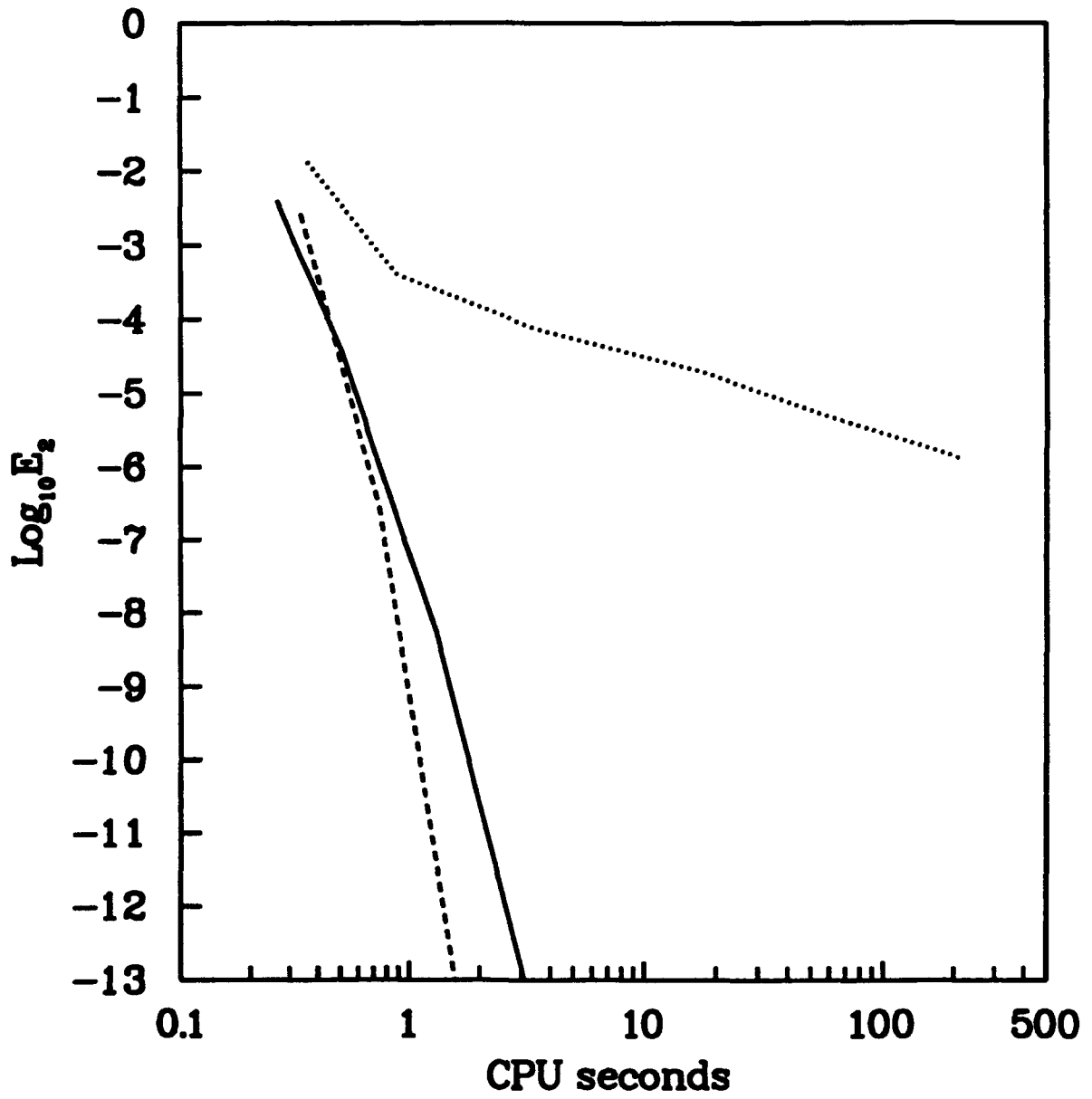


Figure 5

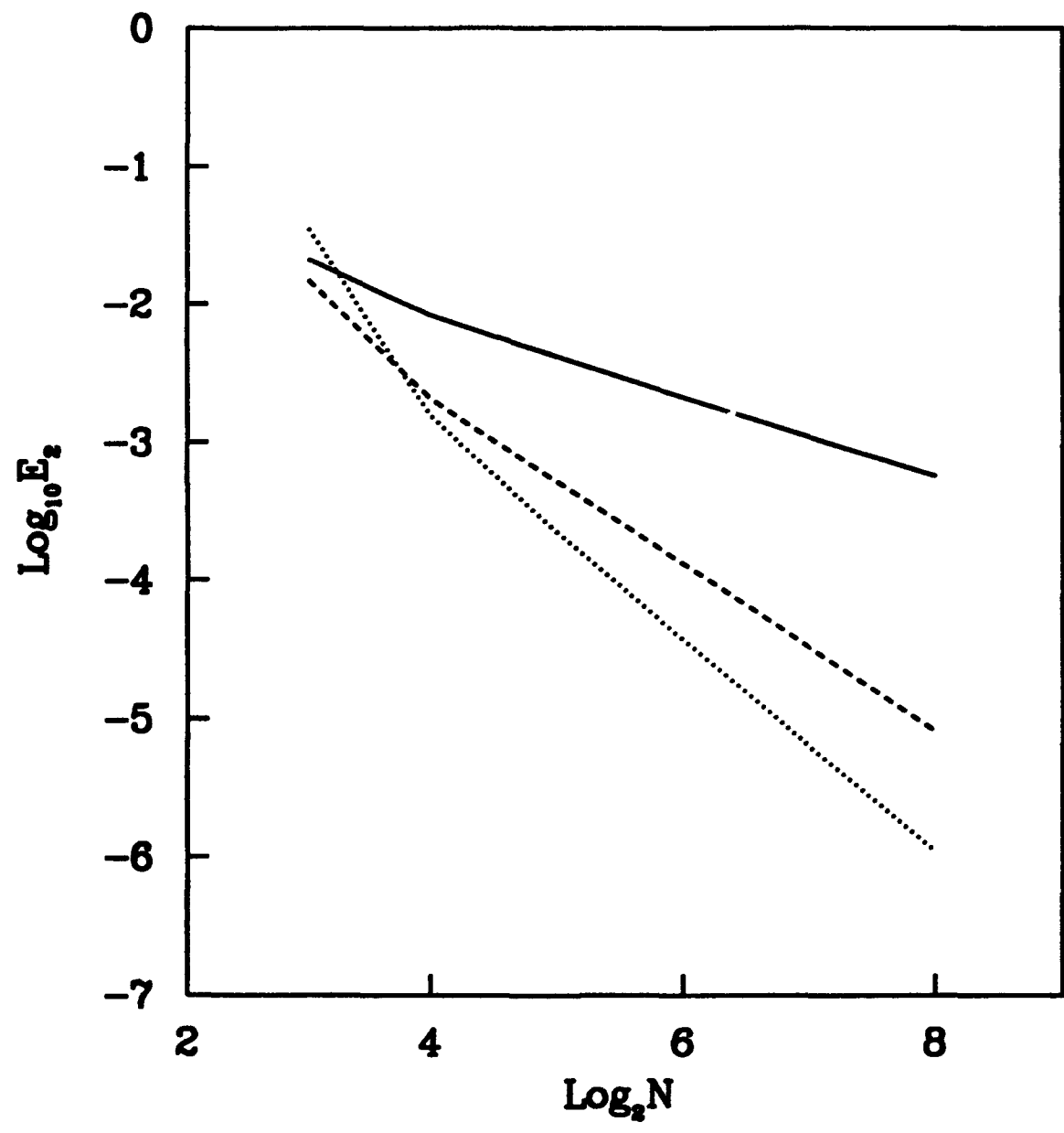


Figure 6

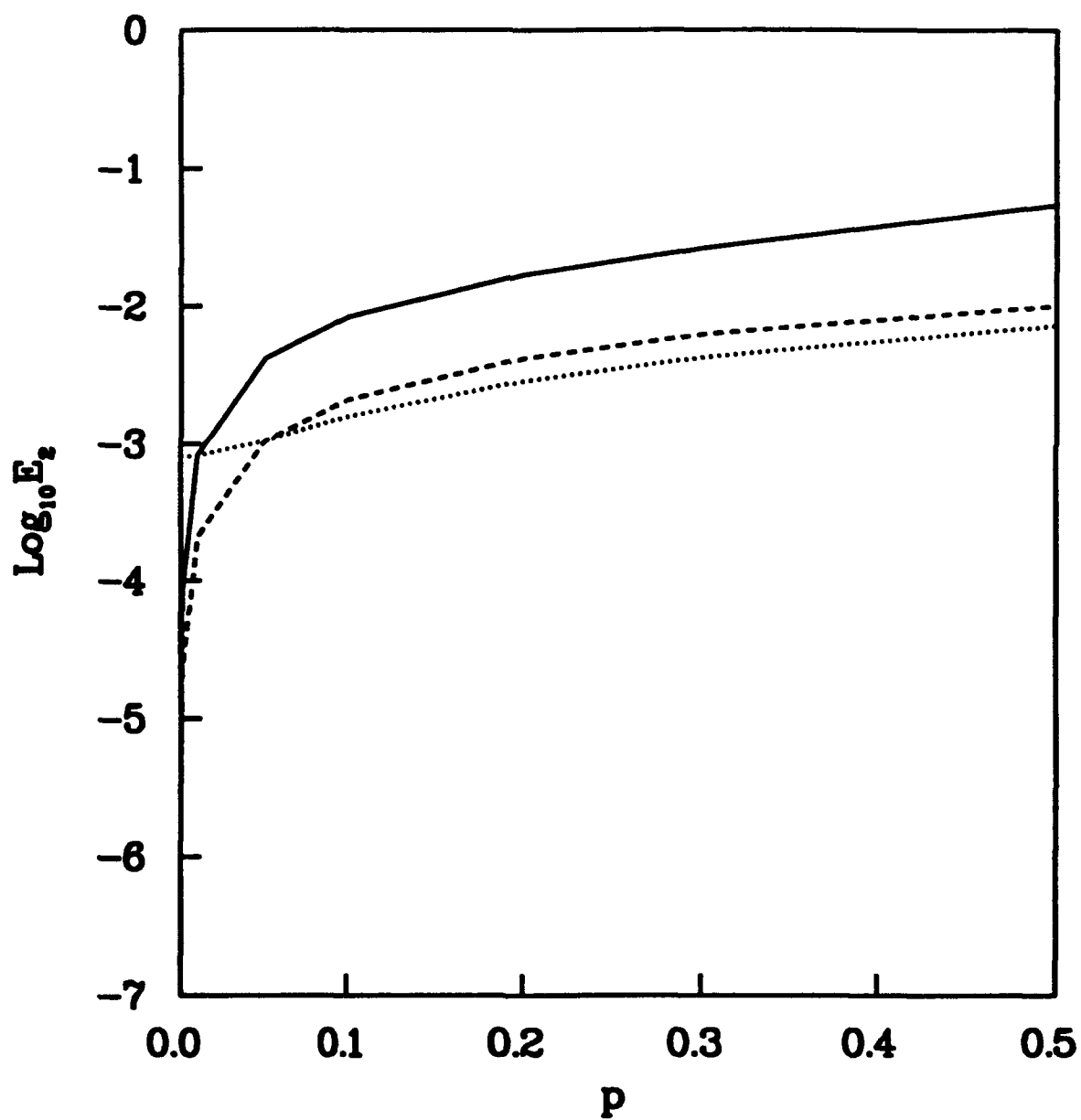


Figure 7

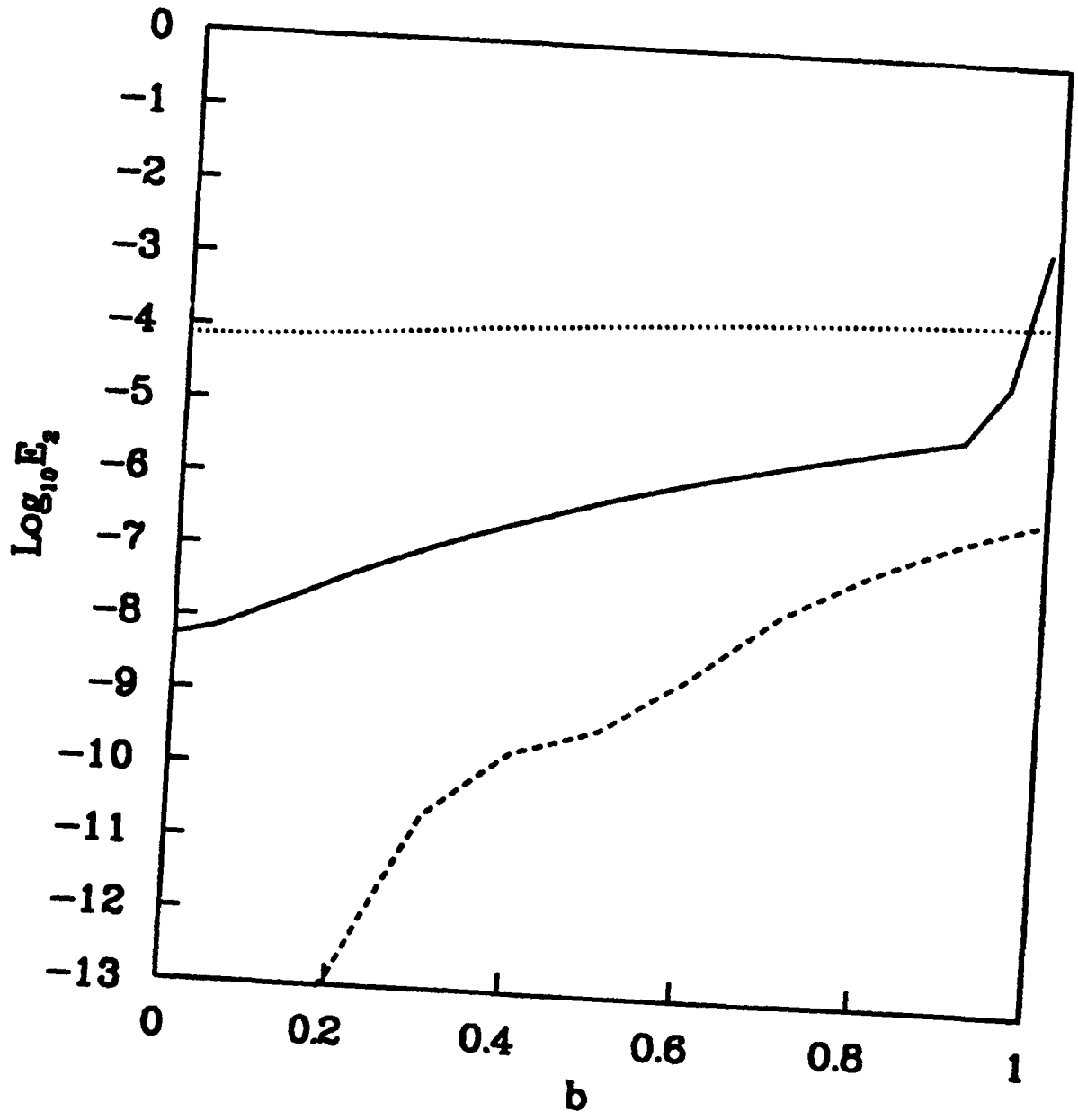


Figure 8

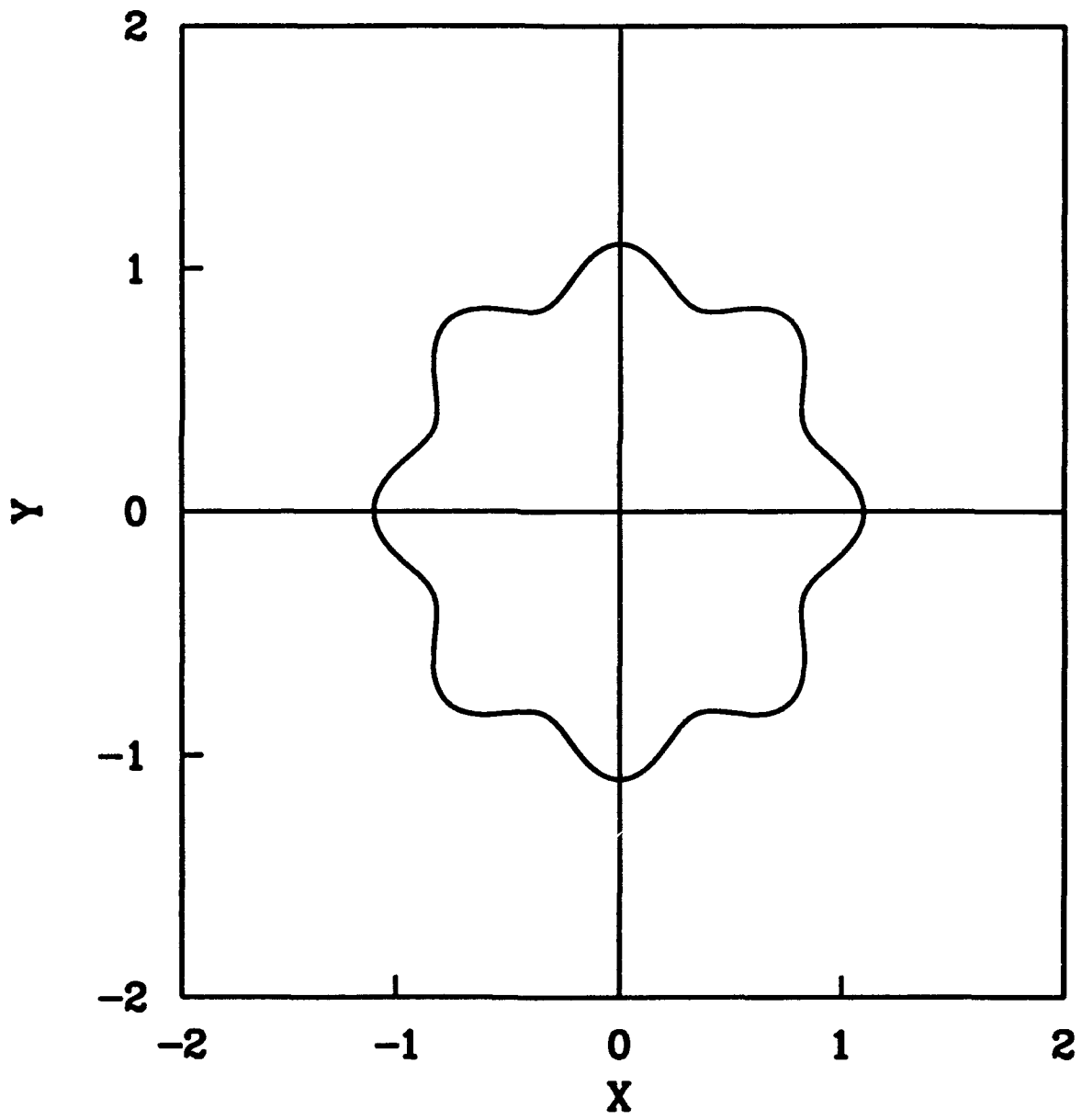


Figure 9

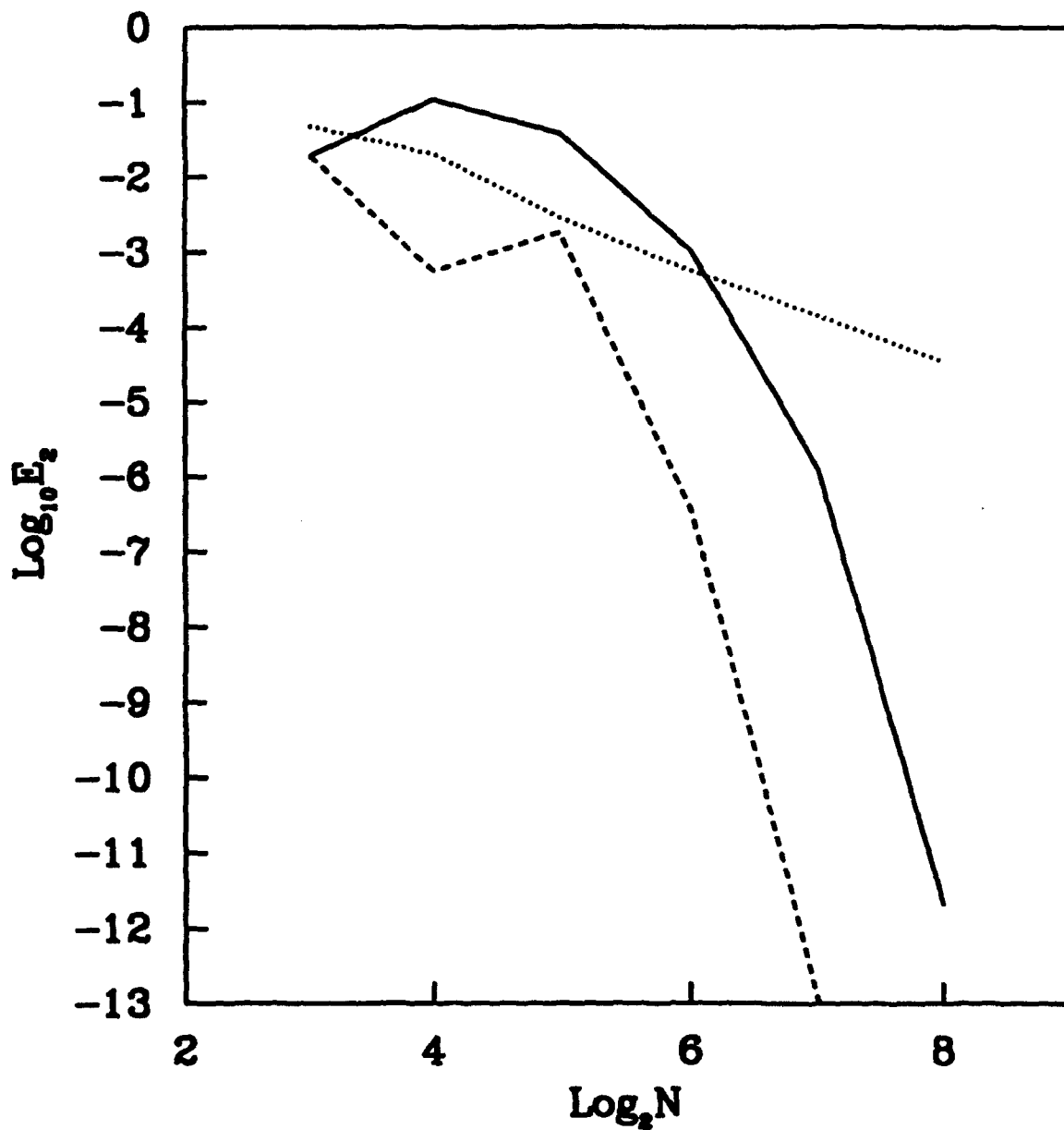


Figure 10

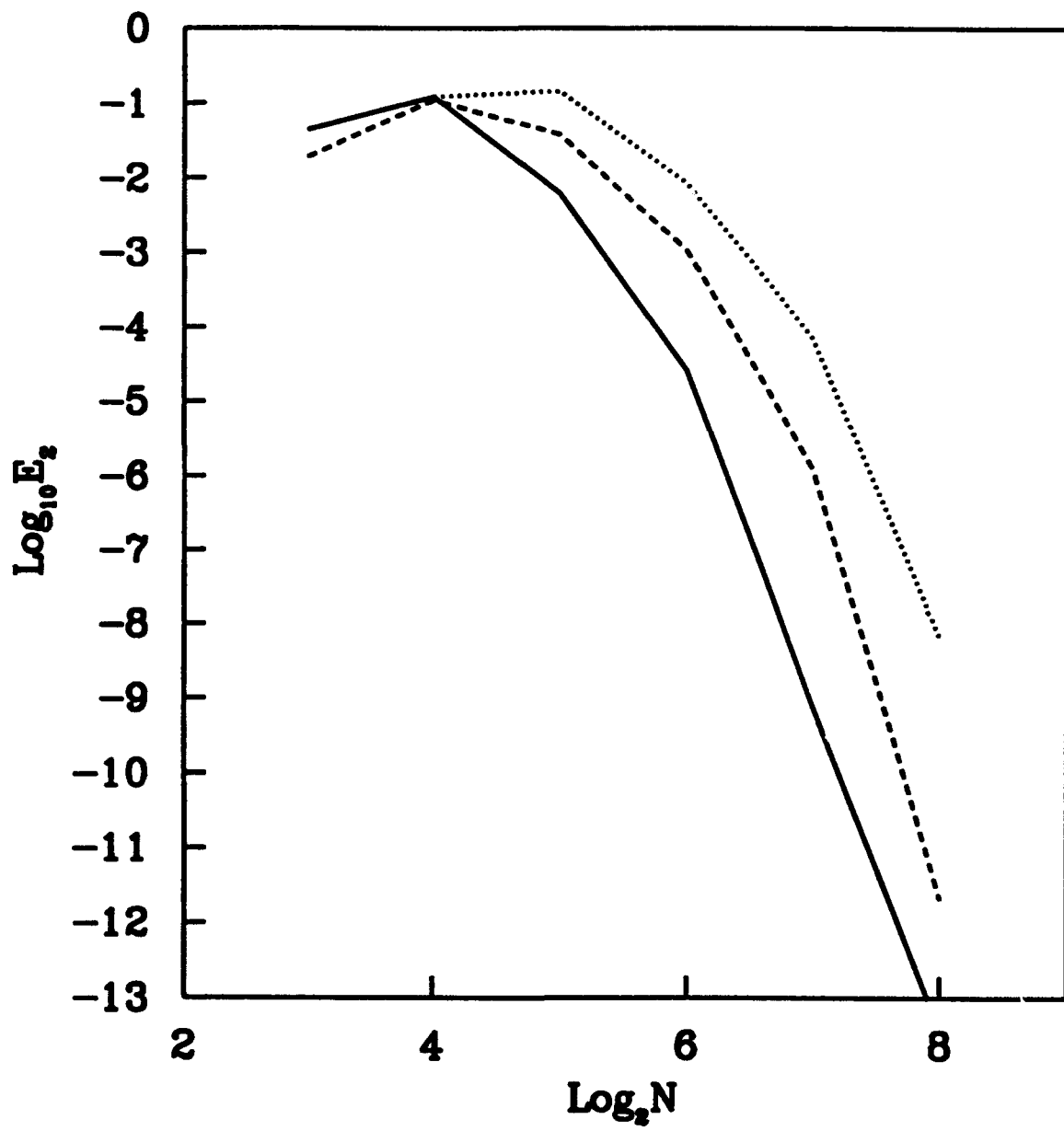
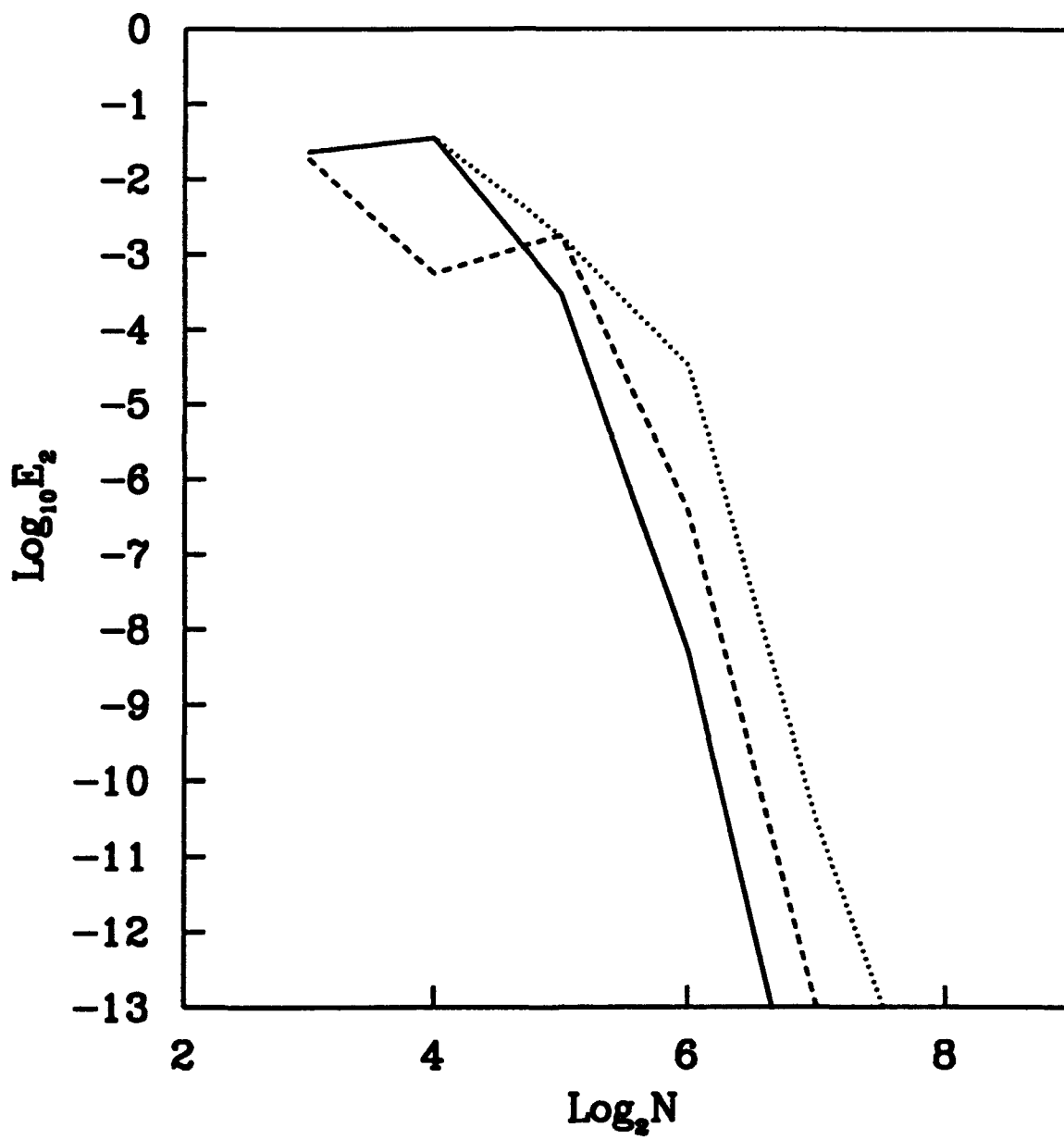


Figure 11



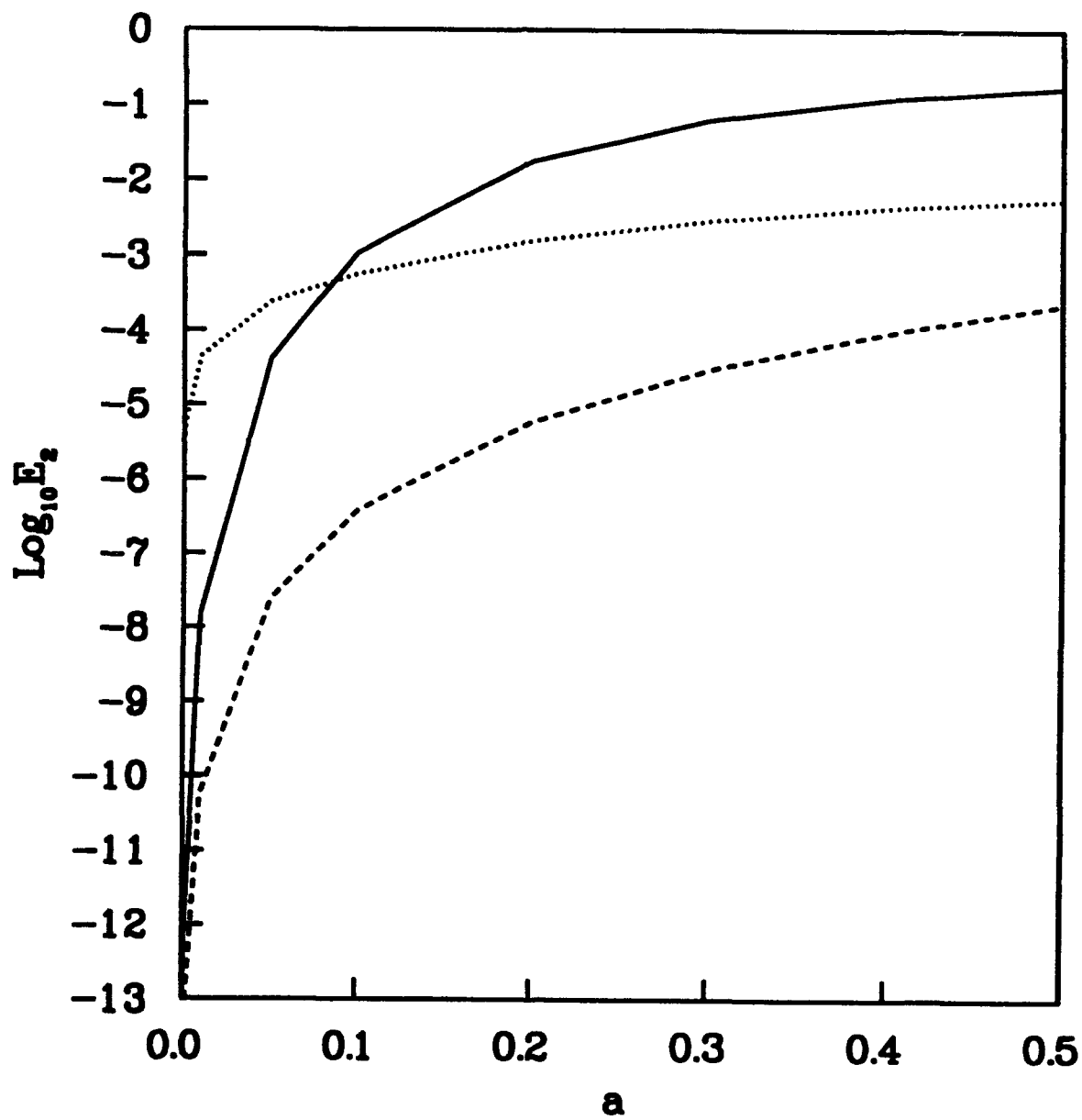


Figure 13

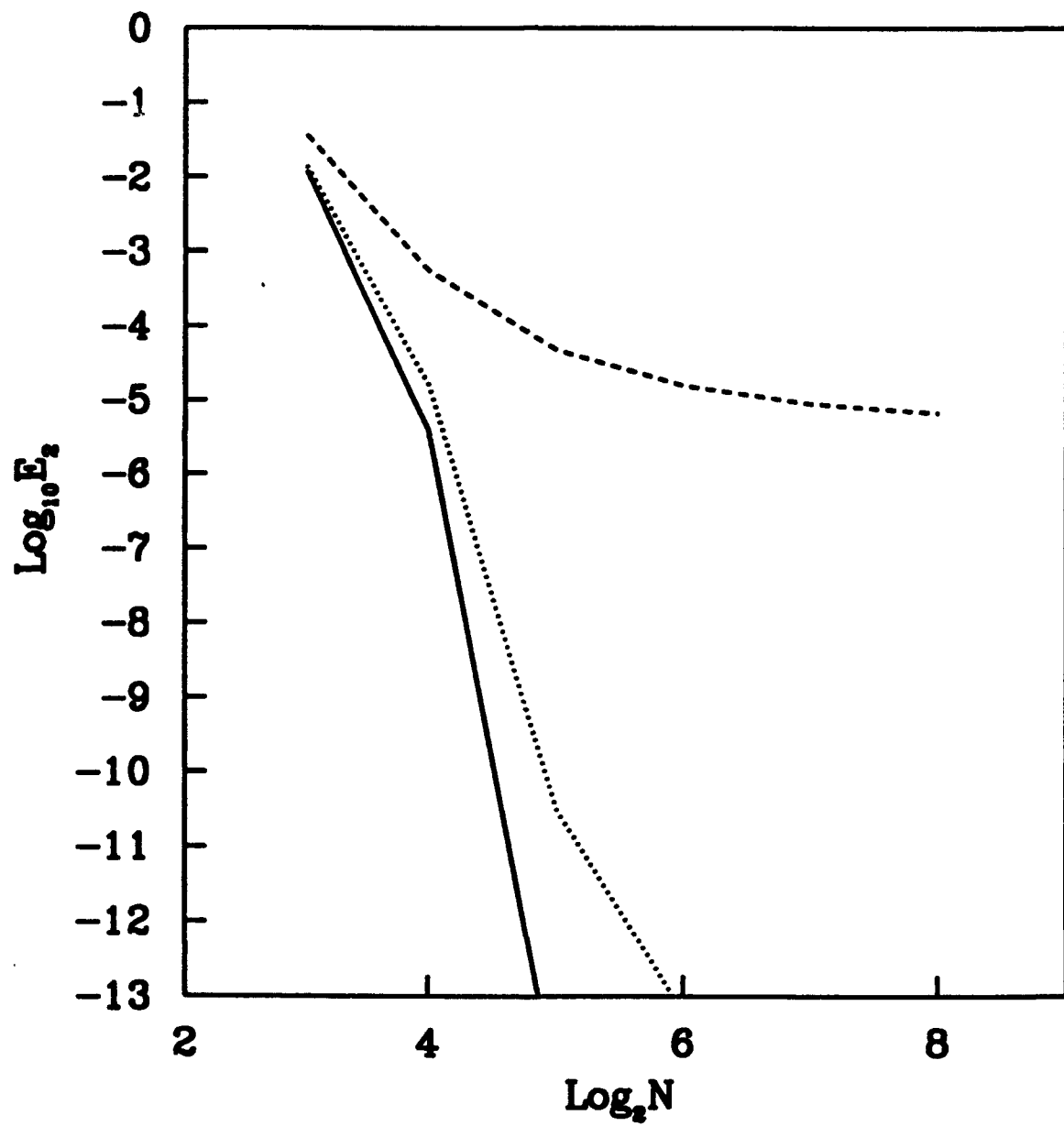


Figure 14

